

Submitted to the Editor of the Astrophysical Journal Letters

Polarimetric Imaging of the Massive Black Hole at the Galactic Center

Benjamin C. Bromley,¹ Fulvio Melia,^{2,3,4} and Siming Liu²

¹Department of Physics, University of Utah, 201 JFB, Salt Lake City, UT 84112

²Physics Department, The University of Arizona, Tucson, AZ 85721

³Steward Observatory, The University of Arizona, Tucson, AZ 85721

Received _____; accepted _____

⁴Sir Thomas Lyle Fellow and Miegunyah Fellow.

ABSTRACT

The radio source Sgr A* in the Galactic center emits a polarized spectrum at millimeter and sub-millimeter wavelengths that is strongly suggestive of relativistic disk accretion onto a massive black hole. We use the well-constrained mass of Sgr A* and a magnetohydrodynamic model of the accretion flow to match both the total flux and polarization from this object. Our results demonstrate explicitly that the shift in the position angle of the polarization vector, seen at wavelengths near the peak of the mm to sub-mm emission from this source, is a signal of relativistic accretion flow in a strong gravitational field. We provide maps of the polarized emission to illustrate how the images of polarized intensity from the vicinity of the black hole would appear in upcoming observations with very long baseline radio interferometers (VLBI). Our results suggest that near-term VLBI observations will be able to directly image the polarized Keplerian portion of the flow near the horizon of the black hole.

Subject headings: accretion—black hole physics—Galaxy: center—hydrodynamics—magnetic fields—radiation mechanisms: non-thermal

1. Introduction

The compact radio source Sgr A* at the Galactic center continues to draw attention from both theorists and observers as the growing body of evidence points more and more to a massive black hole paradigm to explain its characteristics and behavior (for the latest comprehensive review on this subject, see Melia & Falcke 2001). The kinematics of the central star cluster probes the gravitational potential within a mere 0.015 pc of the nucleus and reveals the presence of $2.6 \times 10^6 M_{\odot}$ of dark matter in this region (Genzel et al. 1997; Ghez et al. 1998). Several alternative scenarios invoked to explain this condensation of matter have been excluded with a high degree of confidence (Haller et al. 1996; Genzel et al. 1996; Melia & Coker 1999).

Complementary information on the nature of Sgr A* is provided by its spectral properties, which reflect the physics of matter accreting toward Sgr A* at distances of several Schwarzschild radii ($r_S \equiv 2GM/c^2 \approx 7.7 \times 10^{11}$ cm, or roughly 0.05 A.U.). Falcke, Melia & Agol (2000) have shown that the ‘shadow’ cast by the black hole may have an apparent diameter of about $5r_S$, nearly independent of the black hole spin or its orientation. This depression in intensity (literally, a ‘black hole’) arises from the effects of strong light bending near the event horizon, so that radiation emitted in the background is either absorbed or redirected away from the line-of-sight. The distance to Sgr A* being roughly 8 kpc, this diameter corresponds to an angular size of $\sim 30 \mu\text{as}$, which approaches the resolution of current radio interferometers.

This is very exciting because several aspects of the observational program are evolving toward a fortuitous convergence to make such an important observation feasible within just a few years. No other galactic nucleus, whether in the local and M81 groups, or in the category of very active (though much more distant) sources, can provide such an opportunity in the foreseeable future. Sgr A*’s spectrum at mm/sub-mm wavelengths shows a distinctive ‘hump’ (Falcke et al. 1998), whose characteristics seem to confirm the suggestion that the radiating plasma (emitting predominantly via thermal synchrotron processes) is making a transition from optically thick to thin emission near $\nu = 2 \times 10^{11}$ Hz (Melia 1992, 1994). Other scenarios, such as the jet model (Falcke & Markoff 2000) and the ADAF disk model (Narayan et al 1995), also require that the medium

goes transparent across this range of frequencies. The fortunate aspect about this transition is that it happens to occur at about the same set of frequencies where the scatter broadening in the interstellar medium decreases below the intrinsic source size (see also Melia, Jokipii & Narayanan 1992). Falcke, Melia & Agol (2000) showed that taking this effect into account, as well as the finite achievable telescope resolution, the shadow of Sgr A* should be observable with very long baseline interferometry (VLBI) below ~ 1 mm; it should be quite distinctive at 0.6 mm.

During this past year, considerable progress has been made in modeling the structure and physical attributes of the inner emitting region surrounding Sgr A*, taking into account several crucial new data, including mm/sub-mm polarization measurements (Aitken et al. 2000) and *Chandra's* identification of an X-ray counterpart (Baganoff et al. 2001). In their analysis, Melia, Liu, & Coker (2000, 2001) concluded that the sub-mm bump is probably produced by thermal synchrotron emission in a tight Keplerian flow within the inner $\sim 5 r_S$. A circularization such as this is expected on the basis of hydrodynamical simulations which show that infalling gas possesses an average specific angular momentum to settle into a rotating structure below $\sim 40 r_S$ (Coker & Melia 1997). Presumably the spectrum of Sgr A* longward of $\sim 1 - 2$ mm is generated outside of the Keplerian region, where the gas is making a transition from a quasi-spherical infall into a circularized pattern. Within the rotating plasma, self-Comptonization of the sub-mm bump radiation produces an X-ray component that may account for the *Chandra* source.

Although this correlation between the radio and X-ray components in the spectrum of Sgr A* is not unique to this picture (see, e.g., Falcke & Markoff 2000), the recent detection of significant linear polarization at mm and sub-mm wavelengths (if confirmed) seems to provide supporting evidence for the circularized flow when the flip of the polarization vector is taken into account (Melia, Liu & Coker 2000). The reason for this is that the optically thick emission is dominated by emitting elements on the near and far sides of the black hole, for which the Extraordinary wave (with the magnetic field pointing in the azimuthal direction) has a polarization vector parallel to the reference axis (perpendicular to the Keplerian plane). In contrast, the dominant contribution in the thin region comes from the blue shifted emitter to the side of the black hole, where the

Extraordinary wave has a polarization vector mostly perpendicular to this axis. This is why the position angle apparently shifts by about 90° near the peak of the mm/sub-mm bump.

In this *Letter*, we present the results of new calculations that update these findings in several very important ways, particularly with regard to the upcoming VLBI imaging observations. We have carried out fully self-consistent ray-tracing simulations with the magnetized Keplerian flow geometry to incorporate the effects of light-bending and area amplification into this observationally-motivated physical model. One of our main goals is to produce *polarimetric* images motivated by the expected capability of mm and sub-mm interferometry.

2. Calculation of the Polarimetric Image

Magnetic field dissipation suppresses the field intensity well below its equipartition value in the quasi-spherical portion of the accreting plasma (Kowalenko & Melia 2000). However, once the gas circularizes and settles into a Keplerian flow, a magnetohydrodynamic dynamo can produce an enhanced (though still sub-equipartition) magnetic field, dominated by its azimuthal component (Hawley, Gammie & Balbus 1996). Overcoming the rate of field destruction in the differentially rotating portion of the inflow, the field reaches a saturated intensity since the dynamo time scale is shorter than the dissipation time scale in this region (Melia, Liu & Coker 2001). Our approach in this paper is to consider a physical scenario that seems to account well for all the available data, not only the mm/sub-mm spectrum and degree of polarization, but also the position-angle flip, in order to predict the polarimetric map of Sgr A*. Motivated by certain aspects of earlier hydrodynamical simulations and a pseudo-Newtonian treatment of the inner Keplerian region, and combining these with the phenomenology associated with the salient observational constraints, we are led to adopt a model in which the gas circularizes at small radii, winding the magnetic field within a relativistic Keplerian disk. We take the specific analysis of Melia, Liu, & Coker (2000,2001) to estimate the plausible structure of the gas distribution within several Schwarzschild radii of the black hole, from which we infer the emissivities required to produce the images. We thus track both the Extraordinary and Ordinary waves, which can be expressed, respectively, as

$$\epsilon^e = \frac{\sqrt{3}e^3}{8\pi m_e c^2} B \sin \theta' \int_0^\infty N(E)[F(x) + G(x)] dE, \quad (1)$$

$$\epsilon^o = \frac{\sqrt{3}e^3}{8\pi m_e c^2} B \sin \theta' \int_0^\infty N(E)[F(x) - G(x)] dE, \quad (2)$$

where $N(E)$ is the electron distribution function at energy E , and

$$\cos \theta' = \frac{\cos \theta - v_\phi/c}{1 - (v_\phi/c) \cos \theta}, \quad x = \frac{4\pi\nu m_e^3 c^5}{3eB \sin \theta' E^2}, \quad (3)$$

$$F(x) = x \int_x^\infty K_{5/3}(z) dz, \quad G(x) = x K_{2/3}(x). \quad (4)$$

$K_{5/3}$ and $K_{2/3}$ are the corresponding modified Bessel functions (Pacholczyk 1970). Here, ν is the frequency measured in the co-moving frame, and θ is the angle between the local magnetic field vector and the outward pointing ray. We take a thermal distribution of electrons to fix $N(E)$. (Note that the temperature in this region may reach $\sim 10^{11}$ K, for which inverse Compton processes then produce an X-ray component. We shall not include this in our calculations since we are primarily interested in mapping the polarization vector at mm/sub-mm wavelengths.)

In adopting the model of Melia, Liu, & Coker (2001), we do not fix the parameters a priori, but rather perform a χ^2 -minimization with the goal of producing polarimetric images consistent with the spectral and polarization data. As we shall see, the simulation that produces a good fit to the observed spectrum begins with a gas inflow rate of 3.6×10^{16} g s $^{-1}$, at a circularization radius of $8 r_S$. The light-emitting flow extends down to about $2 r_S$, at which point the gas achieves a plunging orbit into the black hole. Calculating the physical profiles as functions of radius using the prescription in Melia, Liu & Coker (2001), we find that the temperature stays within a factor of a few times 10^{10} K in the Keplerian region, while the particle density varies in the range of about 2×10^7 to 4×10^8 cm $^{-3}$ and the magnetic field increases from about 4 to 20 G. With this model, we find that modestly low inclination angles, around 30° give a good fit to the observations, although higher values are not strongly excluded.

We emphasize that the model parameters adopted here provide a self-consistent description of the flow in the neighborhood of the supermassive black hole. The inflow rate we infer is

substantially lower than the limits obtained using other arguments (e.g., Faraday depolarization), considered within the context of alternative mechanisms for producing the polarized emission (see, e.g., Agol 2000; Quataert & Gruzinov 2000). The viability of the model ultimately depends on the uncertain conditions of the inflow (and, possibly, outflow) at larger radii. For example, the hydrodynamical simulations discussed earlier are rather limited in scope, given that their modest resolution imposed an inner boundary of $1,000r_S$ or more. Thus, there is little guidance as to the behavior of the gas at smaller radii, particularly with regard to whether mass loss occurs or not. Nonetheless, it seems implausible to assume that the specific angular momentum accreted inward of this boundary should increase. At the same time, the heterogeneous nature of the Galactic Center suggests that material arriving in the vicinity of the black will have at least some residual angular momentum, so circularization at small radii seems inevitable.

The overall specific intensity $I_\nu^{e,o}$ observed at infinity is an integration of the emissivity $\epsilon^{e,o}$ over the path length along geodesics. To obtain $I_\nu^{e,o}$ from the emitting accreting disk, we make the simplifying assumption that the disk is geometrically thin, and that its vertical structure is a uniform slab (e.g., Melia, Liu & Coker, 2001). Otherwise, our calculations incorporate all relativistic effects including frame dragging, gravitational redshift, light bending, and Doppler boosting. We use a second-order geodesic solver similar to that introduced by Bromley, Chen & Miller (1997), and trace photon trajectories from a pixel-array detector all the way through a thick spherical shell bounded by the outer disk radius and a surface near the event horizon. We pick up contributions to the observed flux every time the trajectory intersects the disk midplane. In this way, the primary disk image (from photons traveling directly to the observer without crossing the midplane after leaving the disk) and higher-order images (multiple midplane crossings) are formed.

The output of our ray-tracing code is a pixelized image, with specific intensities at the detector calculated from the relativistic invariant I_ν/ν^3 . Emitter-frame frequencies come from the projection of the emitted photon 4-momentum onto the 4-velocity of the emitter (e.g., Cunningham 1975). Similarly, local emission angles, such as θ' in Equation (1), follow from projection of the photon 4-momentum onto the spacelike components of a tetrad tied to the emitter frame. We

assume Keplerian flow except at small radii where circular orbits are unstable. In this case the emitters are on freefall trajectories as if perturbed from the minimum stable orbit ($3 r_S$ for a black hole with zero angular momentum). We calculate fluxes by summing over the pixels in the image, taking into account the physical size of the detector array and the distance to the disk.

The ray-tracing method adopted here is tuned for the synchrotron problem in two novel ways. First, our code is capable of integrating radiative transfer equations along photon trajectories. Here we make only modest use of this feature by allowing for absorption of light from high-order images after multiple disk crossings, taking into account the redshift of photons as they travel from one region of the emitting gas to another. It will be more important to exercise the code’s full capabilities in future work when we treat detailed models of the disk’s vertical structure.

The second key feature of our code is the calculation of polarization in a strongly curved spacetime. It is straightforward to relate the specific intensity of each polarization separately in the emitter and detector frames from the relativistic invariant I_ν/ν^3 , and the degree of polarization is itself an invariant. The position angle of polarized light may also be calculated from a relativistic invariant related to the parallel transport of a polarization vector along a null ray (Connors & Stark 1977; Laor, Netzer & Piran 1991). Here we perform the parallel transport operation quite directly by defining a reference vector at the detector and numerically propagating it along with the null ray itself. This allows us to consistently map a position angle from one frame to another, an essential feature for calculating radiative transfer for the Ordinary and Extraordinary waves that make multiple passes through the disk.

Aitken et al. (2000) provide specific constraints for the magnetohydrodynamic disk model and our relativistic calculations in terms of the total flux and polarization of Sgr A*. The polarization “flip” in the spectrum near a wavelength of 1 mm is a particularly important constraint. We use a nonlinear least-squares search of the model parameter space, including spatial extent of the accretion flow, the mass accretion rate, and other factors governing the radial infall velocity, disk thickness and magnetic field strength (see Melia, Liu & Coker 2001 for details) in order to optimize the fit. Here we consider only a non-rotating black hole. The inclination angle i is

sampled sparsely, but sufficiently to demonstrate that low values of i provide a greater total flux, while high values of i give a sharper polarization flip. As mentioned above we find that $i = 30^\circ$ yields a good fit, although, larger angles are not strongly excluded.

There are strong observational constraints on the linear polarization from Sgr A* at longer wavelengths as well. Bower et al. (1999) have placed limits on the linear polarization at a variety of frequencies below 100 GHz. For our simulations, the 1% upper bound at 86 GHz is the most constraining; at this frequency, our simulation predicts 0.7% linear polarization. The predicted linear polarization at longer wavelengths is $\ll 0.1\%$, consistent with the observationally-imposed limits. Figure 1 shows a comparison between the simulation results and the data.

3. Discussion

The polarimetric images demonstrate that future mm/sub-mm interferometry can directly reveal material flowing near the horizon in Sgr A*. Here, the “shadow” of the black hole takes the form of a dark cavity in a crescent. The bright crescent shape itself, and its highly distinctive distribution of polarized light, may be understood as a manifestation of the relativistic beaming from material on the incoming side of the disk. For optically thin synchrotron emission, the specific intensity in the emitter frame is highly anisotropic, and the beaming effect causes an alignment between the observed photon trajectory and the direction of maximum emission only on the incoming side. This effect is most apparent in the images which show individual components of polarized light. For example, in the absence of relativity the Extraordinary emission will dominate the flux along the disk spin axis where the photon emission and polarization position angles are at 90° to the azimuthal magnetic field. However, the relativistic beaming causes the region of maximum Extraordinary emission to shift toward the incoming side of the disk.

Following Falcke, Melia & Agol (2000) we now assess the possibility that VLBI imaging may reveal the structure of the accretion flow, its polarized emission, and the presence of the event horizon. Figure 2 shows images of the accretion flow at an ideal detector, as well as polarimetric

images taking into account the blurring due to a finite VLBI resolution and scattering by the interstellar medium. The blurring is modeled by convolution with two Gaussians: the first is an approximate model of the scattering effects with an ellipsoidal filter whose major- and minor-axis FWHM values are $24.2 \mu\text{as} \times (\lambda/1.3 \text{ mm})^2$ and $12.8 \mu\text{as} \times (\lambda/1.3 \text{ mm})^2$, respectively, for emission at wavelength λ (Lo et al. 1998). For the purposes of creating test VLBI images, we chose the spin axis of the disk to lie along the minor axis of the scattering ellipsoid, and we have assumed a global interferometer with a 8,000 km baseline (Krichbaum 1996). The second is a spherically symmetric filter with a FWHM of $33.5 \mu\text{as} \times (\lambda/1.3 \text{ mm})$ to account for the resolution effects of an ideal interferometer. These images demonstrate clearly the viability of conducting polarimetric imaging of the black hole at the Galactic center with upcoming VLBI techniques.

Acknowledgments We thank Vladimir Pariev for his suggestions on the polarization calculations in curved spacetime. This research was partially supported by NASA under grants NAG5-8239, NAG5-9205, and NAG5-8277, and has made use of NASA’s Astrophysics Data System Abstract Service. FM is very grateful to the University of Melbourne for a Miegunyah Fellowship. BCB acknowledges computing support from NASA/JPL Supercomputing.

REFERENCES

- Aitken, D.K., Greaves, J., Chrysostomou, A., Jenness, T., Holland, W., Hough, J.H., Pierce-Price, D. & Richer, J. 2000, *ApJ Letters*, 534, L173
- Agol, E. 2000, *ApJ Letters*, 538, L121
- Baganoff, F. et al. 2001, *ApJ*, submitted
- Bower, G.C., Backer, D.C., Zhao, J.-H. et al. 1999, *ApJ*, 521, 582
- Bromley, B.C., Chen, K., & Miller, W.A. 1997, *ApJ*, 475, 57
- Coker, R.F. & Melia, F. 1997, *ApJ Letters*, 488, L149
- Connors, P.A., & Stark, R.F. 1977, *Nature*, 269, 128
- Cummingham, C.T. 1975, *ApJ*, 202, 788
- Falcke, H., Melia, F., & Agol, E. 2000, *ApJ Letters*, 528, L13
- Falcke, H., Goss, WM., Matsuo, H., Teuben, P., Zhao, J-H & Zylka, R. 1998, *ApJ*, 499, 731
- Falcke, H. & Markoff, S. 2000, *A&A*, in press
- Genzel, R., et al. 1996, *ApJ*, **472**, 153.
- Genzel, R., Eckart, A., Ott, T. & Eisenhauer, F. 1997, *MNRAS*, **291**, 219.
- Ghez, A.M., Klein, B.L., Morris, M. & Becklin, E.E. 1998, *ApJ*, 509, 678
- Haller, J.M., et al. 1996, *ApJ*, **456**, 194.
- Hawley, JF., Gammie, CF., Balbus, SA. 1996, *ApJ*, 464, 690
- Kowalenko, V, & Melia, F. 2000, *MNRAS*, 310, 1053

Krichbaum, T. 1996, in *Science with Large Millimeter Arrays*, ed. P.A. Shaver (Berlin: Springer),
96

Laor, A., Netzer, H., & Piran, T., 1990, *MNRAS*, 242, 560

Lo, K.Y., Shen, Z.Q., Zhao, J.H., & Ho, P.T.P. 1998, *ApJ*, 508, L61

Melia, F. 1992, *ApJ Letters*, 387, L25

Melia, F. 1994, *ApJ*, 426, 577

Melia, F. & Coker, R. 1999, *ApJ*, 511, 750

Melia, F. & Falcke, H. 2001, *ARAA*, 39, 309

Melia, F., Jokipii, J.R. & Narayanan, A. 1992, *ApJ Letters*, 395, L87

Melia, F., Liu, S. & Coker, R.F. 2000, *ApJ Letters*, 545, L117

Melia, F., Liu, S. & Coker, R.F. 2001, *ApJ*, in press

Narayan, R., Yi, I. & Mahadevan, R. 1995, *Nature*, 374, 623

Pacholczyk, AG. 1970, *Radio Astrophysics*, (W.H. Freeman and Company: San Francisco)

Quataert, E. & Gruzinov, A. 2000, *ApJ*, 545, 842

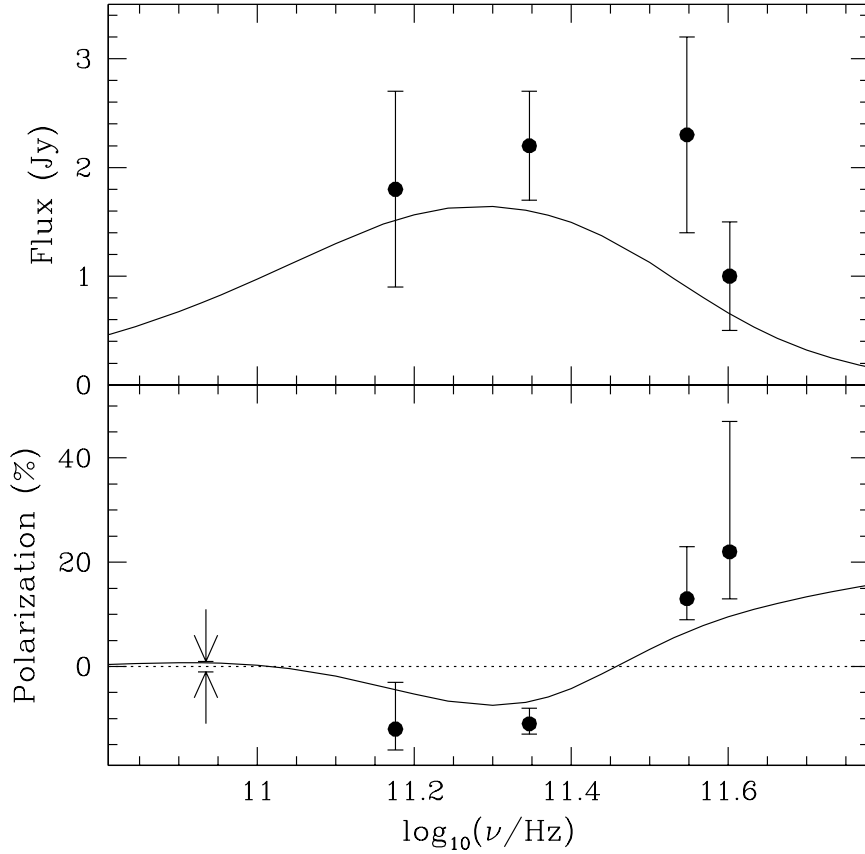


Fig. 1.— Spectra showing total flux density and polarization from Sgr A*. The high-frequency data points are from Aitken et al. (2000) and the curves are from the magnetohydrodynamic model discussed in the text. The limit at 84 GHz is from Bower et al. (1999). At even lower frequencies, the best fit polarization is consistent with 0. In this figure, ‘negative’ polarization corresponds to the polarization vector being aligned with the spin axis of the black hole, whereas positive is for a perpendicular configuration. The polarization crosses 0 when this vector flips by 90° .

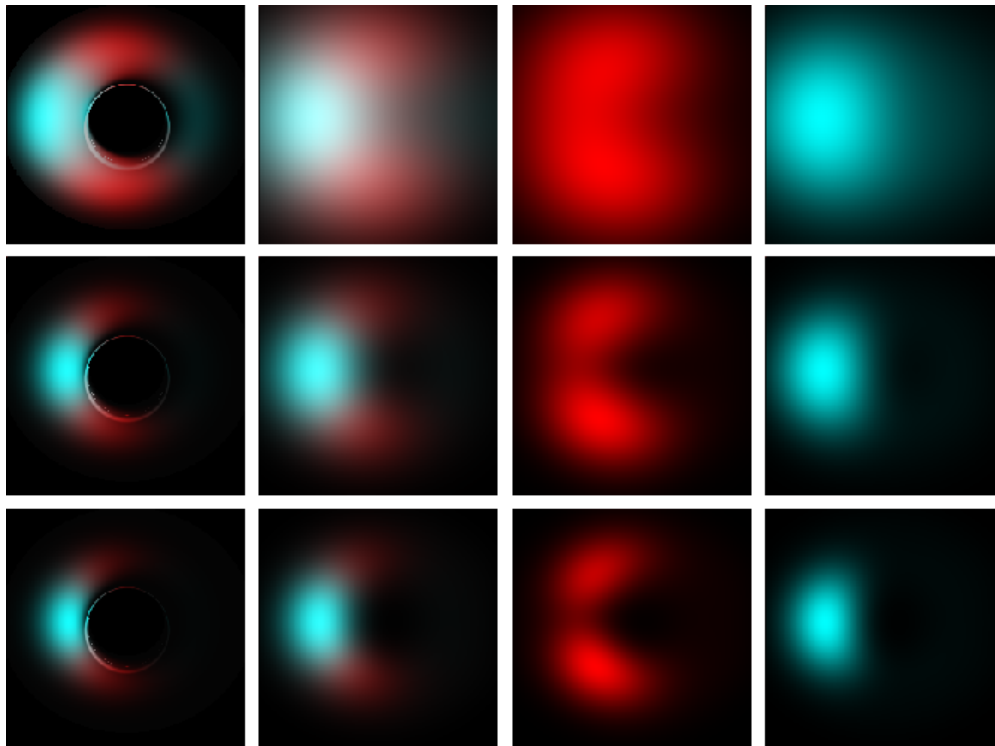


Fig. 2.— Polarization maps at three wavelengths near the peak of the mm to sub-mm emission from Sgr A*. The top row shows emission at 1.5 mm, the middle row is at 1 mm, and the bottom row corresponds to 0.67 mm. The images in each row show the raw ray-tracing output (first column on the left), and an image blurred to account for finite VLBI resolution and interstellar scattering (second column). The two rightmost columns give the vertical and horizontal components of the polarized emission. Throughout, red pixels designate vertically polarized light, and cyan corresponds to horizontal polarization. The pixel brightness in all images scales linearly with flux.